Molecular Vision 2026; 32:370-386 <http://www.molvis.org/molvis/v32/370>
Received 14 March 2025 | Accepted 10 September 2026 | Published 12 September 2026

© 2026 Molecular Vision

Huoxuetongluo formula alleviates diabetic retinopathy by modulating the MEG3/miR-494-5p axis and inhibiting PI3K/AKT/mTOR signaling

Neng Li,[1] Jian Lai,[1] Lin Zhu[2]

[1]Department of Ophthalmology, Hangzhou Hospital of Traditional Chinese Medicine, Hangzhou, China; [2]Department of Ophthalmology, Hangzhou Dingqiao Hospital, Hangzhou, China

Background: Diabetic retinopathy (DR) is a leading cause of blindness. The traditional Huoxuetongluo formula has therapeutic potential, but its specific protective mechanisms against DR remain unclear.
Methods: Huoxuetongluo components were identified via ultra-high-performance liquid chromatography quadrupole time-of-flight mass spectrometry. In diabetic db/db mice, treatment was evaluated by assessing metabolic parameters, retinal damage, apoptosis, inflammation, oxidative stress, and angiogenesis. The expression of miR-494, lncRNA MEG3, and related proteins (PI3K/AKT/mTOR, NOX4, VAV2) was analyzed. In high glucose–induced mouse retinal microvascular endothelial cells, treatment with 10% drug-containing serum and transfection with shRNA-MEG3 or miR-494–5p mimic were performed. Cellular assays included viability, proliferation, permeability, tube formation, and dual-luciferase reporter validation of the MEG3/miR-494–5p interaction. Gene and protein expression changes were confirmed by quantitative real-time PCR and western blot.
Results: Huoxuetongluo, containing 181 components primarily composed of flavonoids, effectively reduced body weight and fasting blood glucose, improved retinal structure, normalized lipid metabolism, and alleviated apoptosis in diabetic mice. Furthermore, it attenuated oxidative stress, inflammation, and angiogenesis by downregulating the PI3K/AKT/mTOR pathway, upregulating lncRNA MEG3, and suppressing miR-494. Cellular experiments demonstrated that Huoxuetongluo treatment reversed high glucose–induced dysregulation of lncRNA MEG3 and miR-494–5p, suppressed PI3K/AKT/mTOR pathway activation, and ameliorated endothelial dysfunction. Rescue experiments and dual-luciferase reporter assays confirmed that its protective effects are mediated through the MEG3/miR-494–5p regulatory axis.
Conclusions: Huoxuetongluo exerts protective effects against DR by modulating the MEG3/miR-494–5p axis and inhibiting the PI3K/AKT/mTOR signaling pathway.

Diabetic retinopathy (DR) is the leading microvascular complication of diabetes and the most common cause of blindness among adults aged 20 to 74 years [1–3]. Its pathogenesis involves a complex interplay of inflammation, oxidative stress, and dysregulated signaling pathways. Oxidative stress triggers an inflammatory response by increasing reactive oxygen species (ROS) production, leading to DNA damage and apoptosis. Inflammatory factors such as interleukins and tumor necrosis factor are elevated in the DR, disrupting the blood–retinal barrier and promoting vascular damage and pathologic angiogenesis. In addition, alterations in signaling pathways, such as activation of nuclear factor κB, further exacerbate the inflammatory response and apoptosis [4]. Furthermore, inflammation also promotes the development of DR and retinal damage by modulating immune responses, activating glial cells, impairing vascular function, and inducing macular edema [5]. Notably, DR manifests earlier and with greater severity in patients with type 1 than in type 2 diabetes. Currently, the treatments for DR include laser therapy, vitrectomy, and drugs. As for drugs, it mainly involves corresponding intervention for the specific symptoms of DR. Antihypertensive drugs to control blood pressure to significantly reduce fundus fluorescence leakage; lipid-regulating drugs can be used can significantly slow the progression of retinopathy with dyslipidemia; dimethyl fumarate drugs have a significant protective effect against high glucose–induced retinal pigment epithelial cell damage by reducing the inflammatory cascade [6–9]. However, these treatments just relieve some symptoms caused by DR. Therefore, it is crucial to thoroughly explore the pathogenesis of DR and seek a corresponding therapeutic method for the disease.

The pathogenesis is complex owing to the various mechanisms leading to the DR. The research manifests that the pathogenesis of retinopathy is mainly regulated by diverse pathways, including those related to cellular metabolism, signaling, and growth factor effects. The pathways involved include polyol pathway activation and accumulation of

Correspondence to: Jian Lai, Department of Ophthalmology, Hangzhou Hospital of Traditional Chinese Medicine, No. 453, Stadium Road, Xihu District, Hangzhou, Zhejiang, 310007, China; Phone: +86-0571-85827552; FAX: +86-0571-85827894; ORCID: 0009-0000-4993-0231; email: laijian318@126.com

advanced glycation end products, oxidative stress, protein kinase C activation, inflammation, the renin–angiotensin system, and vascular endothelial growth factor (VEGF) upregulation, all of which collectively lead to the destruction of the blood–retinal barrier [10]. Recent studies have shown that the expression of long noncoding RNA maternally expressed gene 3 (lncRNA MEG3) is significantly associated with type 2 diabetes mellitus [11]. Tu et al. [12] found that the expression level of lncRNA MEG3 was significantly downregulated in DR mice and endothelial cells. It does not affect the total expression level of any protein but causes increased retinal angiogenesis and may aggravate vascular leakage and inflammation [13]. The phosphoinositol 3 kinase (PI3K)/protein kinase B (AKT)/mammalian target of rapamycin (mTOR) signaling pathway is involved in a series of metabolic processes such as glucose transport, glycogen protein synthesis, and decomposition in the life activities of cells. During the occurrence and development of diabetes, persistent hyperglycemia can promote the activation of the PI3K/AKT/mTOR signaling pathway, which in turn causes the activation of phosphorylated PI3K/AKT/mTOR signaling in various cells due to lncRNA MEG3 knockdown, ultimately accelerating the development of DR [14,15]. Therefore, lncRNA MEG3 upregulation is likely to become an important direction for the treatment of DR.

Traditional Chinese medicine holds that obstruction of blood circulation causes disease in the eyes. A previous study showed that Huoxuetongluo (HXTL) has obvious effects on dilating blood vessels, accelerating blood flow and increasing blood flow, inhibiting fibrous tissue hyperplasia, eliminating microcirculation disorders, further correcting glucose and lipid metabolism in patients with DR, and alleviating systemic microvascular complications [16]. In addition, clinical research has demonstrated the safety and tolerability of HXTL in humans [17]. Our research obtained HXTL through the compatibility of traditional Chinese medicine, which consists of *Astragalus*, *chuanxiong*, *Angelica*, *Radix Paeoniae Rubra*, peach kernel, safflower, *Salvia miltiorrhiza* Bge., *Pueraria*, *Retinervus Luffae Fructus, Curcuma*, *Acorus*, leech, motherwort, *Lycopi herba*, and honeysuckle. However, research on the effects of HXTL in DR remains preliminary, and its specific mechanisms are still unclear. Furthermore, studies on the optimal dosage of HXTL for DR treatment have not yet been reported.

Our previous study found that HXTL acted effectively to improve the symptoms of DR and discovered that the expression of lncRNA MEG3 in the retina was significantly lower than that in DR mice treated with HXTL. These observations support the hypothesis that HXTL can be used to treat DR. Therefore, this study was designed to examine whether HXTL alleviates DR by modulating oxidative stress and angiogenesis in db/db mice, as well as explore its molecular mechanism involving the MEG3/miR-494–5p axis and the PI3K/AKT/mTOR pathway.

METHODS

Animals: Forty male BKS-db$^{-/-}$ mice of specific pathogen–free grade, weighing 45 ± 4 g, were obtained in littermates, with 10 male BKS-db$^{+/+}$ thin mice weighing (25 ± 6) g in the control group, all purchased from Shanghai SLAC Laboratory Animal Co. (Shanghai, China; animal production license number: SCXK (Hu) 2017–0005). Six male C57BL/6 mice aged 6 to 8 weeks were also purchased from Shanghai SLAC Laboratory Animal Co. (license: SCXK (Hu) 2022–0004). The rearing temperature was 22–25 °C, and the humidity was 50% to 80%. The mice were subjected to artificial 12-h/12-h circadian light. The animal experiments were performed in accordance with the regulations of the Institutional Animal Care and Use Committee. The animal research was ratified by the Ethics Committee of the Animal Center of Zhejiang Eyong Pharmaceutical Research and Development Center (animal use license number: SYXK (Zhe) 2021–0033). The animals were fed adaptively for a week before the start of the whole experiment.

HXTL prescription: The prescription for HXTL is composed of *Astragalus* 10 g, *chuanxiong* 10 g, *Angelica* 12 g, *Radix Paeoniae Rubra* 5 g, peach kernel 5 g, safflower 5 g, *S. miltiorrhiza* Bge. 18 g, *Pueraria* 10 g, *Retinervus Luffae Fructus* 12 g, *Curcuma* 10 g, *Acorus* 10 g, leech 5 g, motherwort 10 g, *L. herba* 12 g, and *honeysuckle* 5 g.

Ultra-high-performance liquid chromatography quadrupole time-of-flight mass spectrometry analysis: Approximately 200 mg of the sample was weighed and mixed with a precooled methanol/acetonitrile/water (2:2:1, v/v) solution. The mixture was thoroughly homogenized and then subjected to ultrasonic extraction for 30 min. Following extraction, the mixture was centrifuged at 23,000 ×g for 5 min, and the supernatant was collected. The supernatant was concentrated to dryness under vacuum and reconstituted in 200 µl of 50% methanol solution. For the analysis, a Nexera X2 LC-30AD UPLC system (Shimadzu, Kyoto, Japan) was employed. Then, the sample was separated on an ACQUITY UPLC (Milford, MA) HSS T3 column (2.1 × 100 mm, 1.8 µm). The mobile phase consisted of 0.1% formic acid in water (A) and 0.1% formic acid in acetonitrile (B) with the following gradient elution program: 0 to 17.5 min, 3% to 90% B; 17.5 to 21 min, maintain 90% B; 21 to 22 min, 90% to 3% B; and 22 to 25 min, maintain 3% B. The injection volume was 5 µl,

the column temperature was maintained at 40 °C, the flow rate was set at 0.4 ml/min, and the sample tray temperature was kept at 8 °C.

The TurboIonSpray ion source was used for electrospray ionization, with scanning performed in both positive and negative ion modes. The ion source parameters were set as follows: both gas I and gas II pressures were set to 55 psi, the curtain gas flow rate was 35 l/min, and the ion source temperature was maintained at 550 °C. The ion spray voltage was set to 5,500 V in positive ion mode and −4,500 V in negative ion mode. The scanning range for the time-of-flight mass spectrometry was set to 50 to 1,500 Da, and the product ion scanning range was 25 to 1,000 Da. Data acquisition and processing were performed using SCIEX OS software (Marlborough, MA).

Animal grouping and administration: After adaptive feeding for 1 week, 40 db/db mice were randomly divided into the following groups: diabetes model group, HXTL low-dose group, HXTL medium-dose group, HXTL high-dose group, and metformin group (200 mg/kg) by random. Metformin was chosen as the positive control based on previous studies indicating its common use in DR treatment and its efficacy at 200 mg/kg in regulating angiogenic and anti-inflammatory factors in type 2 diabetic mice [18,19]; as a result, we use it as a positive control group. Considering the dose conversion between humans and mice, through the calculation, the middle dose of HXTL was 21 g/kg, low dose was 10.5 g/kg, and high dose was 42 g/kg. The DR group and the control group were given 0.9% sodium chloride solution by intragastric administration. The gavage lasted for 8 weeks. The administration group began treatment after the modeling was successful. The whole experimental flowchart is presented in Figure 1.

Detection of animal body weight and fasting blood glucose of mice: The body weight and fasting blood glucose (FBG) of mice in each group were measured and recorded every 2 weeks after the administration, and the body weights of each group were recorded using an electronic balance. The animals were fasted for 8 h, then the blood was punctured through the tail vein and collected on the blood glucose test paper. FBG levels were immediately analyzed using a glucometer, and the results were recorded.

Lipid metabolism measurement: Eight weeks after administration, mice in each group were fasted overnight, and blood was collected from the orbital sinus, incubated at 37 °C for 30 min, centrifuged at 3,000 rpm for 10 min, and the serum was separated. The contents of total cholesterol (TC), triglyceride (TG), low-density lipoprotein cholesterol (LDL-C), and high-density lipoprotein cholesterol (HDL-C) of serum were detected by an automatic biochemical analyzer.

Hematoxylin and eosin staining: The mice were anesthetized with isoflurane. The eyeballs were quickly removed and fixed with 4% paraformaldehyde. The eyeballs were dehydrated by gradient ethanol and xylene, then immersed in wax. The tissues were cut into 5-μm slices and affixed to the antipeeling slides. The slices were baked at 60 °C for 12 h, dewaxed and hydrated by xylene and gradient ethanol, and stained with a hematoxylin stain (MDL, Beijing, China; MD911467) and eosin stain (BASO, Zhuhai, China; 613101). Finally, ethanol with a low to high concentration was added to dehydrate. The samples were vitrified with xylene, then sealed with neutral balsam and observed under the microscope.

Immunohistochemistry assay: The prepared paraffin sections of retinal tissue were dewaxed with xylene. Then, ethanol was successively added with a high to low concentration to rehydrate the tissue, and antigen repair solution was added.

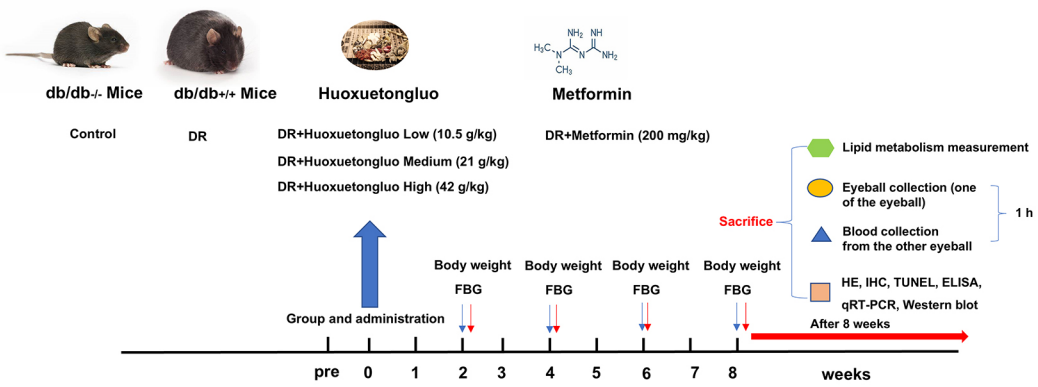


Figure 1. Experimental flowchart. FBG: fasting blood glucose; DR: diabetic retinopathy; HE: hematoxylin-eosin; IHC: immunohistochemistry; ELISA: enzyme-linked immunosorbent assay; qRT-PCR: quantitative real time-PCR.

Next, the sections were washed with hydrogen peroxide to block endogenous peroxidase and later sealed with bovine serum and incubated overnight with 3-nitrotyrosine (3-NT; Proteintech, Rosemont, IL 18,084-1-AP), CD31 (Novus, Lone Tree, CO; AF3628), 4-hydroxynonenal (4-HNE; Abcam, Cambridge, UK, ab48506), vascular endothelial growth factor receptor (VEGFR; Proteintech, 26,415-1-AP), TNF-α (Abcam, ab307164), SOD (Affinity, Changzhou, China; AF5144), and 8-OHdG (Abcam, ab48508) at 4 °C. On the second day, the corresponding secondary antibody of horseradish peroxidase (HRP) was incubated. DAB (SERVICEBIO, Wuhan, China; G1211) was added. The positive expression of DAB was brown-yellow, and the nuclei were stained with hematoxylin. Finally, ethanol at low to high concentrations was added to dehydrate and vitrify with xylene. The slices were sealed with neutral balsam and were observed under a microscope.

Enzyme-linked immunosorbent assay measurement: Mouse retinal tissues were collected and immediately homogenized, and a specified volume of phosphate-buffered saline was added. The homogenate was further ground on ice until thoroughly processed, followed by centrifugation at 5,000 ×*g* for 10 min to collect the supernatant. An enzyme-linked immunosorbent assay (ELISA) was performed according to the manufacturer's instructions. The absorbance (OD) of each well was subsequently measured at a 450-nm wavelength. The kits used, including interleukin-1β (IL-1β; mouse, ml063132), vascular endothelial growth factor (VEGF; mouse, ml002076), and 8-hydroxy-2 deoxyguanosine (8-OHdG; mouse, ml002198), were determined using ELISA kits (Shanghai Enzyme Linked Biotechnology Co., Shanghai, China), as well as homocysteine (Hcy; CUSABIO, Wuhan, China; mouse, CSB-E16551m), superoxide dismutase (SOD; Shanghai Biyuntian Biotechnology Co., Shanghai, China; S0101S), and malonaldehyde (MDA; Nanjing Jiancheng Biologic Engineering Research Institute Co., Nanjing, China; A003–1-2) following the manufacturers' instructions.

TdT-mediated dUTP nick-end labeling staining: TdT-mediated dUTP nick-end labeling (TUNEL) staining was performed using a one-step TUNEL cell apoptosis detection kit (Beyotime, Shanghai, China, C1090). The positive cell rate was calculated as the number of apoptotic cells divided by the total cell count, multiplied by 100%.

Cell culture and establishment of a high glucose–induced cell model: Mouse retinal microvascular endothelial cells (mRMECs; ICell Bioscience, Shanghai, China) were digested with 0.25% trypsin containing 0.01% EDTA, observed under an inverted microscope and harvested approximately 3 min after rounding. The cell suspension was seeded at 2 × 10^5 cells/25 cm^2 and cultured at 37 °C with 5% CO_2. After 48 h, the medium was replaced with M200 medium containing 1% fetal bovine serum, which was subsequently refreshed every 2 to 3 days. Cells from passages 3 to 6 were used for experiments. A diabetic cell model was established by treatment with medium supplemented with 25 mM glucose [20].

Preparation of 10% drug-containing serum: HXTL was administered to six healthy male C57BL/6 mice at a dose of 42 g/kg (calculated based on human-to-animal dose conversion, serum dilution ratio, and clinical dosage) twice daily (0.2 ml per administration) for 3 consecutive days via gavage. One hour after the last administration, blood was collected and centrifuged at 23,000 ×g for 15 min at 4 °C. Serum was filtered through a 0.22-μm filter, heat-inactivated at 56 °C for 30 min, and stored at −80 °C until use. The HXTL-treated cells were cultured in medium supplemented with 10% drug-containing serum [21].

Cell transfection: Transfection was performed using Lipofectamine 3000 (Thermo Fisher Scientific, Waltham, MA, L3000008). shRNA-MEG3 carried by a lentiviral vector and miR-494–5p mimics were used to knock down MEG3 and overexpress miR-494–5p, respectively [22]. High glucose–induced mRMECs were transfected accordingly, with untransfected cells serving as blank controls.

Cell grouping and administration: mRMECs were divided into the following seven groups: a normal control group (treated with 5.5 mM glucose medium) and six groups cultured under high glucose (25 mM glucose) conditions: high glucose (HG) group, HG + HXTL group (supplemented with 10% drug-containing serum of HXTL), HG + HXTL + MEG3-KD group (additionally transfected with shRNA-MEG3), HG + HXTL + miR-494–mimic group (additionally transfected with miR-494–5p mimics), HG + MEG3-KD group (transfected with shRNA-MEG3 only), and HG + miR-494–mimic group (transfected with miR-494–5p mimics only).

Quantitative real-time PCR: Total RNA was extracted from retinal tissue and mRMECs using Trizol (Sangon Biotech, Shanghai, China, B511311) and transcribed into complementary DNA (cDNA) with a reverse transcription kit (Jiangsu Cowin Biotech, Jiangsu Province, China; CW2569). Primers, DEPC, cDNA and SYBR Green (Takara, Shiga, Japan; RR820A) were added to prepare the corresponding system for amplification products in the PCR instrument. In performing the quantitative PCR (qPCR) reaction, we used the following cycling conditions: first an initial denaturation at 95 °C for 10 min to ensure adequate unwinding of the template DNA, followed by denaturation at 95 °C for 15 s and then annealing and extension at 60 °C for 60 s to complete

Table 1. Primer sequences.

Gene	Forward primer (5′-3′)	Reverse primer (5′-3′)
Mouse IL-6	GGCGGATCGGATGTTGTGAT	GGACCCCAGACAATCGGTTG
Mouse IL-1β	TTGAAGTTGACGGACCCCAA	TGTCCTGACCACTGTTGTTTC
Mouse TNF-α	TCACTGGAGCCTCGAATGTC	TCTGTGAGAAGGCTGTGCA
Mouse GAPDH	TCAACGGCACAGTCAAGG	TGAGCCCTTCCACGATG
Mouse miR-494	ACTTGAAGGAGAGGTTGTCCG	AAAAGAGGTTTCCCGTGTATGT
Mouse lncRNA MEG3	GGTCTGAGTTCTATTGCCAGC	CAGGGACACATACACTGCCTT
Mouse U6	ATGGGTCGAAGTCGTAGCC	TTCTCGGCGTCTTCTTTCTCG

a cycle. Such cycling conditions were repeated a total of 40 times to ensure adequate amplification of the target gene. Mouse primer sequences are listed as Table 1. Fold changes of messenger RNA (mRNA) were calculated according to the $2^{-\Delta\Delta CT}$ method.

Western blot: Pure protein was extracted from retinal tissue and mRMECs, and protein concentration was measured by the bicinchoninic acid (BCA) method. After loading, the buffer was added, and the protein was boiled to induce denaturation. Total proteins were separated by electrophoresis using 10% sodium dodecyl sulfate–polyacrylamide gel electrophoresis, and the corresponding proteins were transferred to a polyvinylidene fluoride membrane. The nonspecific antigen was blocked with 5% milk, and the protein on the membrane was incubated with the target antibodies nicotinamide adenine dinucleotide phosphate oxidase 4 (NOX4; DF6924, 1:1,000), guanine nucleotide exchange factor 2 (VAV2; AF9228, 1:1,000), p-PI3K (AF3242, 1:1,000), PI3K (AF6241, 1:1,000), p-AKT (AF0016, 1:1,000), AKT (AF6261, 1:1,000), p-mTOR (AF3308, 1:1,000), mTOR (AF6308, 1:1,000), and β-actin (AF7018, 1:10,000) all from Affinity. After overnight incubation at 4 °C, unbound antibodies were washed with Tris-buffered saline and Tween, then incubated with anti-rabbit IgG and HRP-linked secondary antibodies (7074, 1:6,000; Cell Signaling Technology, Danvers, MA) at room temperature for 1 h. Unbound antibodies were washed again and captured in an electrochemiluminescence (ECL) luminescence imager.

Cell viability assay: The viability of mRMECs was assessed using the cell counting kit-8 (CCK-8, Beyotime, C0039) according to the manufacturer's instructions [23,24].

5-Ethynyl-2'-deoxyuridine staining: The proliferative activity of retinal microvascular endothelial cells was measured using a BeyoClick EdU-594 cell proliferation detection kit (Beyotime, C0078S) according to the manufacturer's instructions [22].

Luciferase reporter assay: The wild-type and mutant MEG3 sequences were cloned into the psiCHECK-2 vector to construct reporter plasmids. After overnight culture in 96-well plates, cells were cotransfected with the reporter plasmids and miR-494–5p mimics or controls using Lipofectamine 3000. Forty-eight hours after transfection, firefly and *Renilla* luciferase activities were sequentially measured using a dual-luciferase reporter assay system, followed by data analysis.

Transendothelial permeability assay: Human retinal microvascular endothelial cells (HRMECs) were seeded in Transwell inserts and cultured to confluence, followed by respective treatments according to experimental groups. At the endpoint, FITC-dextran (40 kDa, 0.5 mg/ml) was added to the upper chamber. After 6 h, aliquots were collected from both chambers, and fluorescence intensity was measured using a microplate reader. Endothelial monolayer permeability was calculated as the mean rate of FITC-dextran transendothelial exchange (%FD40 = fluorescence intensity in the lower chamber/fluorescence intensity in the upper chamber).

Tube formation assay: Matrigel was thawed overnight at 4 °C. Precooled 96-well plates were coated with 50 µl Matrigel per well (avoiding bubbles) and polymerized at 37 °C for 45 min. After treatment, according to the experimental groups, mRMECs were suspended and seeded at 3.5×10^4 cells per well (50 µl) in triplicate. Following 4-h incubation at 37 °C, images were captured, and tube-like structures were quantified using ImageJ software (National Institutes of Health, Bethesda, MD).

Statistical analysis: The statistical analysis was performed using SPSS software (16.0; SPSS, Inc., Chicago, IL). If the measurement data in multiple groups were in accordance with normal distribution and the homogeneity of variance test, one-way analysis of variance was used, and the Tukey test was used for further pairwise comparisons between groups. Dunnett's T3 test or the independent sample *t* test was used if the distribution was normal but the variance was

not uniform. If it did not conform to the normal distribution, the Kruskal–Wallis *H* test was used. The significance level was α = 0.05. The data were expressed as mean ± standard deviation. $p < 0.05$ was designated as statistically significant.

RESULTS

Identified chemical components in HXTL: The components of HXTL were analyzed using ultra-high-performance liquid chromatography quadrupole time-of-flight mass spectrometry (UPLC-Q-TOF/MS), and chromatograms in both positive and negative ion modes were obtained, as presented in Figure 2A,B. Through data matching, a total of 181 chemical components were identified, with flavonoids and their glycosides being the most abundant, including 20 flavonoids and 20 flavonoid glycosides. Detailed information on all identified compounds is provided in Appendix 1 and Appendix 2.

The effect of HXTL on the body weight, FBG, and lipid metabolism of the mice: To evaluate the therapeutic potential of HXTL in DR mice, we measured body weight, FBG, and lipid metabolism in all mice over 8 weeks, with the metformin group serving as the positive control. From Figure 2C, we found that the HXTL group mice's body weight decreased in a dose-dependent manner compared to the DR mice ($p < 0.05$). Consistently, HXTL downregulated FBG in a dose-dependent manner in the DR mice as well (Figure 2D, $p < 0.05$). Moreover, we discovered that HXTL reduced the levels of TC, TG, and LDL-C; meanwhile, it increased HDL-C (Figure 2E-H, $p < 0.01$), indicating a significant modulation of lipid metabolism. However, HXTL at a low dose showed no difference in adjusting HDL-C and LDL-C compared with the DR group.

The effect of HXTL on histopathologic damage of diabetic retinal tissues in mice: To further validate whether the HXTL repairs the histopathologic damage in diabetic retinal tissues of mice, hematoxylin and eosin (HE) staining was used to confirm this. In the control group, the structure of all retinal layers was intact, the inner boundary membrane was intact and clear, and the capillary was not dilated and congested. On the contrary, the DR group was characterized by incomplete and unclear retinal layer structure, loose edema, sparse cells, a reduced number of retinal ganglion cells, and cells swollen with telangiectasia and hyperemia. The retinal structure of the HXTL group was clearer, the tissue edema was significantly relieved, the cells were more closely arranged, the shape was more regular, and the telangiectasia was reduced (Figure 3A).

The effect of HXTL on angiogenesis and cell apoptosis of diabetic retinal tissues in mice: To evaluate the effects of the HXTL on neovascularization, we stained for CD31 and VEGFR to demonstrate angiogenesis in diabetic retinal tissues in mice. As shown in Figure 3B-D, the immunohistochemistry (IHC) assay confirmed that the positive expressions of CD31 and VEGFR in retinal tissues in mice were notably weakened by HXTL.

In Figure 4A,B, with the TUNEL kit, we found that in the DR group, the TUNEL-positive cell rate was much higher than that of the control group ($p < 0.01$). In addition, among the different dosages of HXTL treated in DR mice, the medium and high dosages alleviated cell apoptosis ($p < 0.01$). In addition, we found that serum VEGF decreased in a dose-dependent manner with HXTL treatment (Figure 4C).

The effect of HXTL on the inflammatory factors of the serum of diabetic retinal tissues in mice: To clarify whether HXTL has anti-inflammatory effects in DR mice, we investigated the serum levels of inflammatory factors such as Hcy and IL-1β using ELISA kits. The data showed that in the DR group, the levels of Hcy, IL-1β, and TNF-α were elevated, while HXTL downregulated serum Hcy and IL-1β, as well as IL-1β and TNF-α in retinal tissues, in a dose-dependent way (Figure 4D-G, $p < 0.05$). In addition, HXTL suppressed the mRNA expression levels of IL-1β, IL-6, and TNF-α in the diabetic retinal tissues in the same way (Figure 4hH-J, $p < 0.05$), whereas low-dose HXTL showed no significant difference compared with the DR group.

The effect of HXTL on oxidative stress of diabetic retinal tissues in mice: To explore whether HXTL alleviates oxidative stress in diabetic retinal tissues in mice, we measured the levels of 3-NT, 4-HNE, SOD, MDA, and 8-OHdG. The results suggested that the positive expressions of 3-NT and 4-HNE were reduced after the treatment of HXTL and metformin (Figure 5A-C). Additionally, HXTL and metformin groups regulated the SOD, MDA, and 8-OHdG levels. Among these, the content of SOD was promoted (Figure 5D, $p < 0.05$), and the content of MDA and 8-OHdG was restrained compared to the DR mice (Figure 5E-F, $p < 0.05$). As shown in Figure 5G-I, the treatments of HXTL and metformin resulted in the reduction of the NOX4 and VAV2 protein expression levels in diabetic retinal tissues of DR mice ($p < 0.05$).

In addition, to further confirm the mitigating effect of HXTL on DR inflammatory response and oxidative stress, we used an IHC assay to examine the expression levels of key biomarkers, such as TNF-α, SOD, and 8-OHdG, in the retinal tissues of mice (Figure 6A-D). The results showed that the average optical density (AOD) values of TNF-α and 8-OHdG were significantly decreased ($p < 0.05$) and the AOD values of SOD were significantly increased ($p < 0.01$) in the retinal tissues of mice in all dose groups of HXTL and metformin groups, as compared with DR.

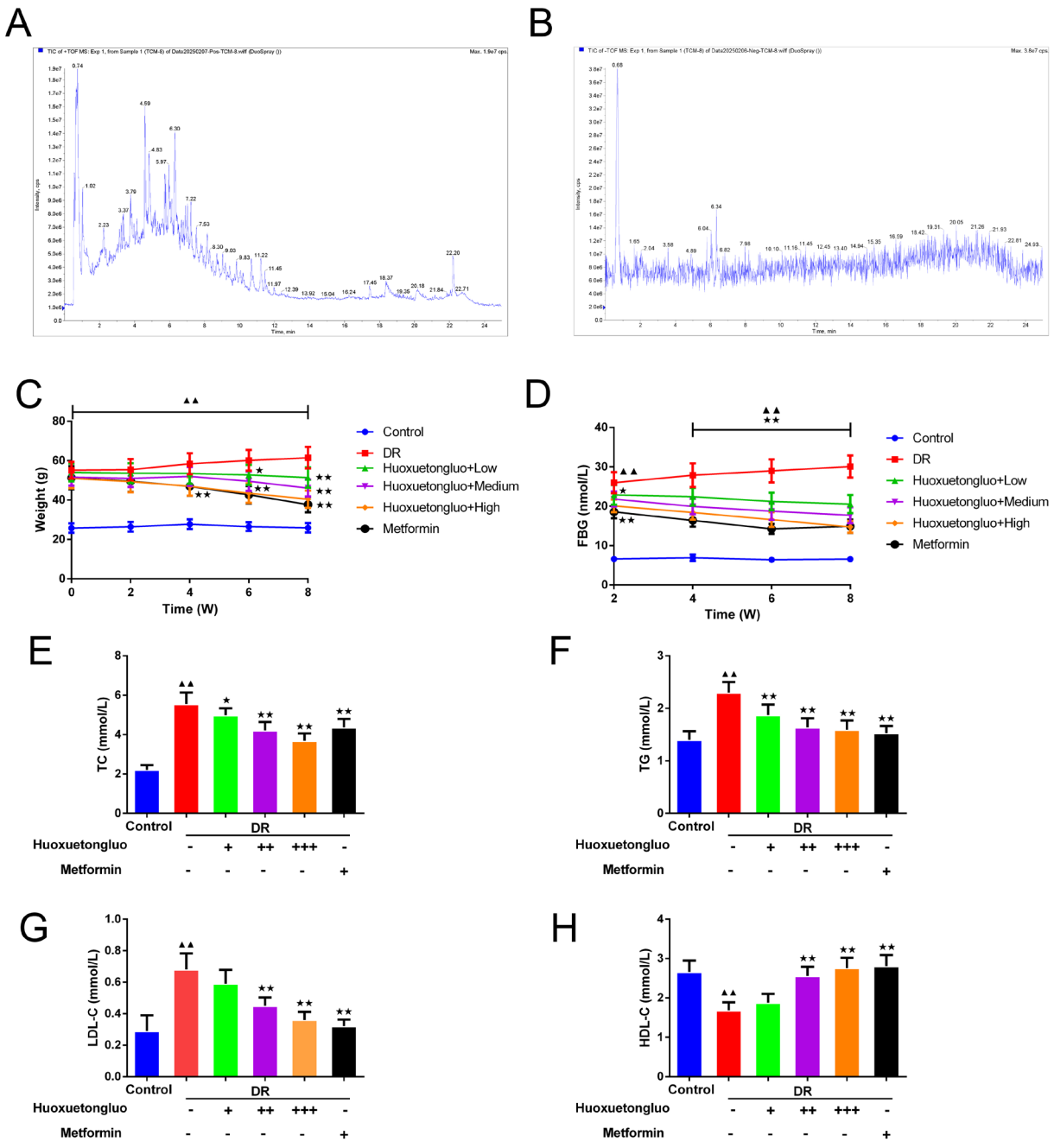


Figure 2. Chemical composition and metabolic effects of HXTL in DR mice. **A**, **B**: UPLC-Q-TOF/MS total ion chromatograms of HXTL in positive (**A**) and negative (**B**) ion modes; **C**: Bodyweight growth curve of mice in each group during 8 weeks of drug treatment, n=10; **D**: FBG of mice in each group, n=10; **E**-**H**: ELISA was used for testing TC, TG, LDL-C, HDL-C levels of the DR mice lipid metabolism in each group. n=10. ▲▲p<0.01 versus control group. ★p<0.05, ★★p<0.01 versus DR group. HXTL: Huoxuetongluo, UPLC-Q/TOF-MS: Ultra-high performance liquid chromatography-quadrupole-time of flight-mass spectrometry, TC: total cholesterol, TG: triglyceride, LDL-C: low-density lipoprotein cholesterol, HDL-C: high-density lipoprotein cholesterol.

The effect of HXTL on the PI3K/AKT/mTOR pathway and lncRNA MEG3 and miR-494 in diabetic retinal tissues of mice: To deeply explore the likely regulated mechanism of the HXTL on DR mice, western blot was used to validate our hypothesis. In our study, results confirmed that HXTL attenuated p-PI3K, p-AKT, and p-mTOR levels of diabetic retinal tissues in mice as well as the ratios of p-PI3K/PI3K, p-AKT/AKT, and p-mTOR/mTOR (Figure 6E-H, $p < 0.05$). To identify the exact molecular pathway involved in regulation, we use quantitative real-time PCR (qRT-PCR) to assess

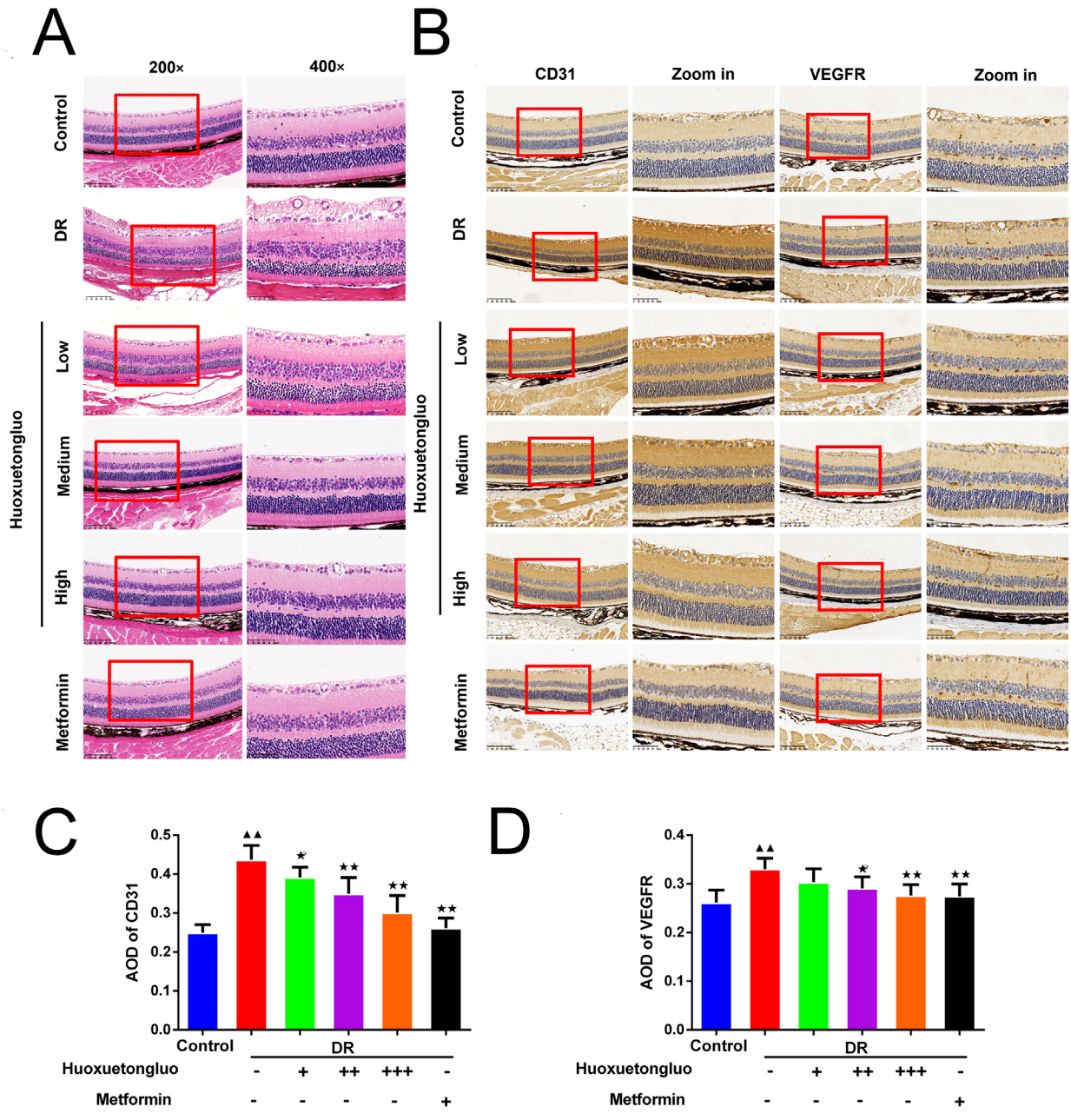


Figure 3. The effect of HXTL on histopathological damage and angiogenesis of DR in mice. **A**: The histomorphology of diabetic retinal tissues in mice was observed by HE staining (magnification × 200, scale bar: 100 μm; magnification × 400, scale bar: 50 μm); **B**-**D**: The positive expressions of CD31 and VEGFR of diabetic retinal tissues in mice were examined by IHC (magnification × 200, scale bar: 100 μm; magnification × 400, scale bar: 50 μm). VEGFR: vascular endothelial growth factor receptor.

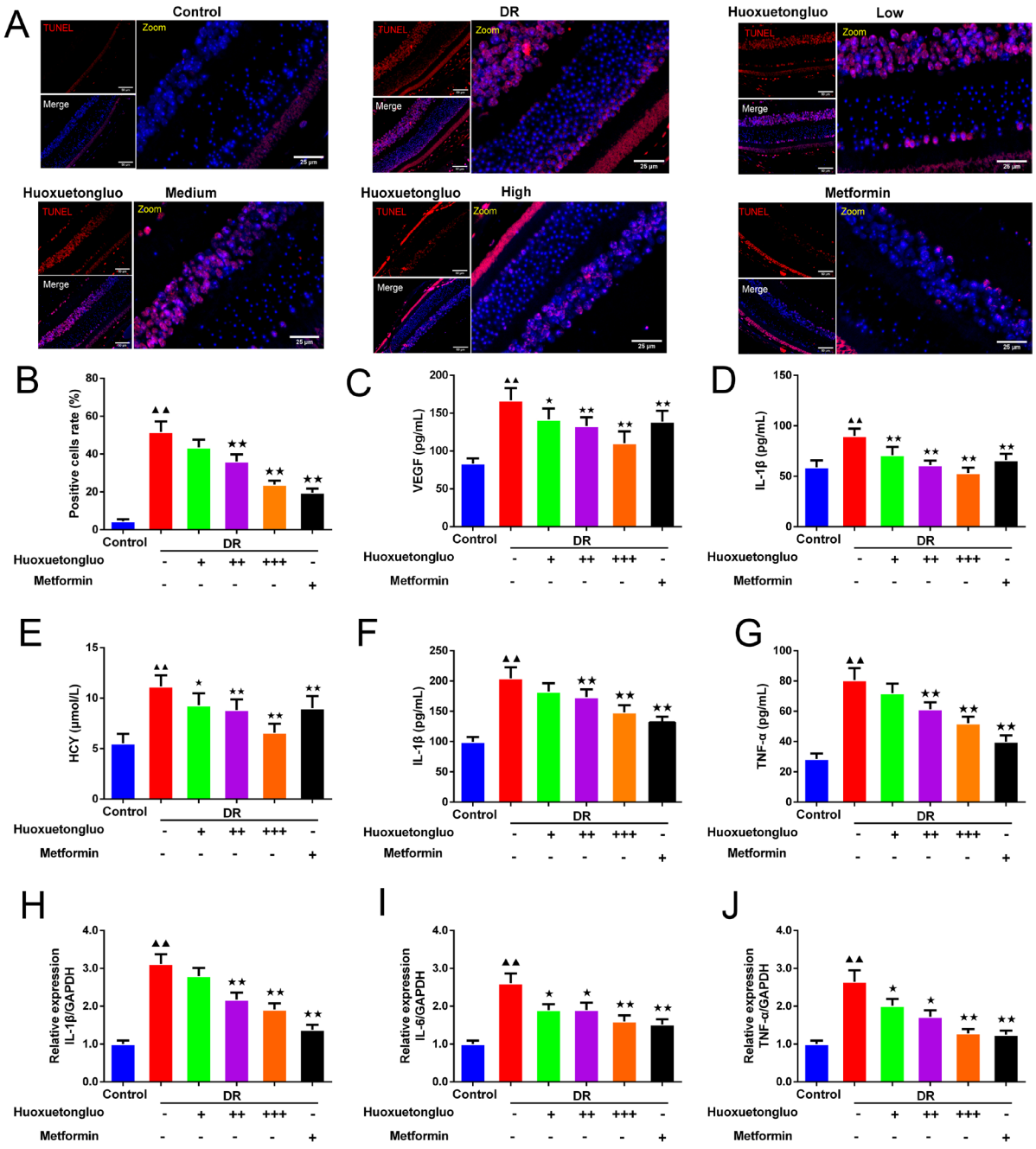


Figure 4. Effects of HXTL on apoptosis, VEGF expression, and inflammatory factors in DR mice. **A**, **B**: Representative images (**A**) and quantification (**B**) of TUNEL-positive apoptotic cells in retinal tissues (magnification × 200, scale bar: 50 μm; magnification × 400, scale bar: 25 μm), n=3; **F-G**: ELISA was used for testing VEGF level (c), IL-1β (**D**) and Hcy (**E**) in serum and IL-1β (f), TNF-α (**G**) in retinal tissues of mice in each group, n=6; **H-J**: qRT-PCR was used for testing IL-1β, IL-6, TNF-α levels of the mice in each group, n=3; ▲▲p<0.01 versus control group, □p<0.05, □□p<0.01 versus DR group. TUNEL: TdT-mediated dUTP nick-end labeling, VEGF: vascular endothelial growth factor, IL-1β: interleukin-1 beta, Hcy: homocysteine, TNF-α: tumor necrosis factor-α.

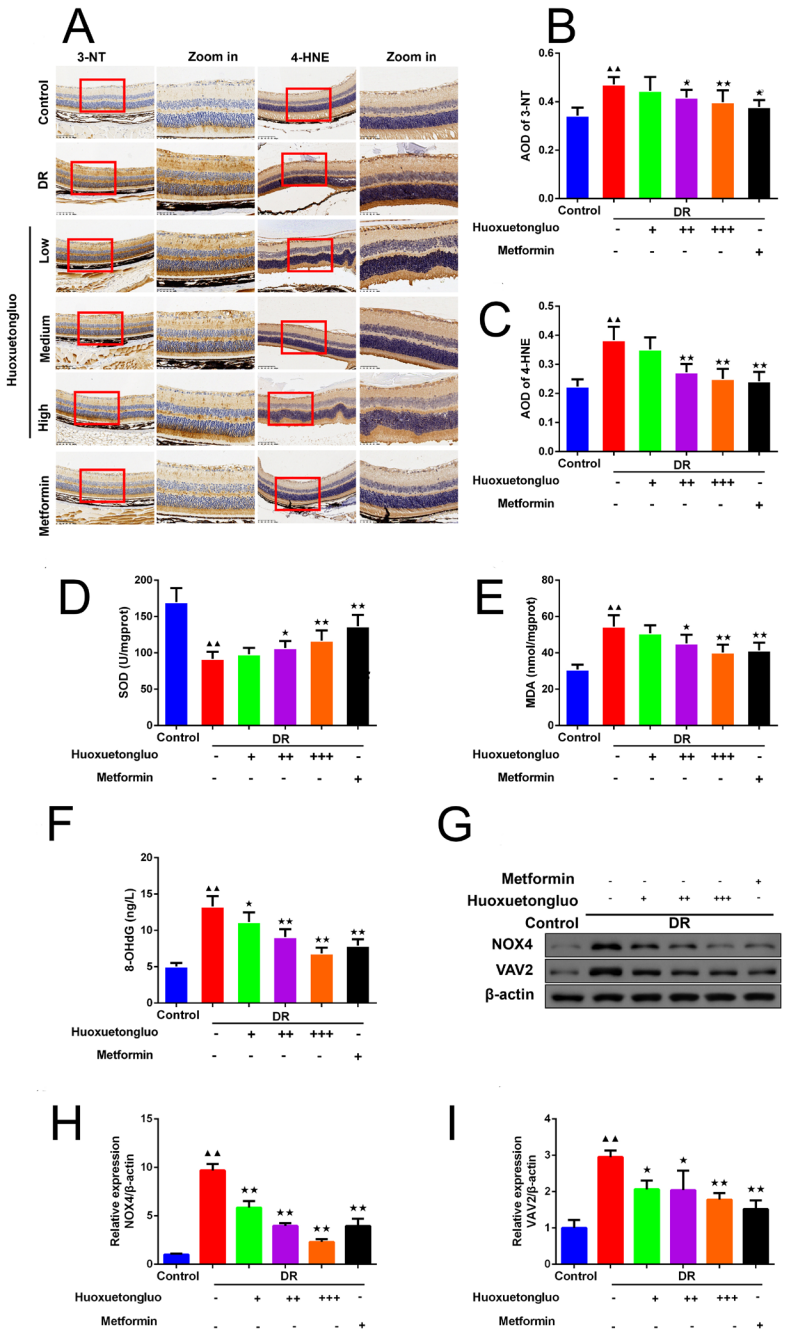


Figure 5. The effect of HXTL on oxidative stress in serum of DR in mice. **A-C**: The positive expressions of 3-NT and 4-HNE of diabetic retinal tissues in mice were examined by IHC (magnification × 200, scale bar: 100 μm; magnification × 400, scale bar: 50 μm). **D-F**: Biochemical kit was used for testing SOD, MDA, 8-OHdG levels in serum of mice in each group, n=6; **G-I**: Western Blot was used for testing NOX4 and VAV2 levels of the mice in each group, n=3; ▲▲p<0.01 versus control group, □p<0.05, □□p<0.01 versus DR group. 3-NT: 3-nitrotyrosine, 4-HNE: 4-hydroxynonenal, SOD: superoxide dismutase, MDA: malonaldehyde, 8-OHdG: 8-hydroxy-2 deoxyguanosine, NOX4: Nicotinamide Adenine Dinucleotide Phosphate Oxidase 4, VAV2: guanine nucleotide exchange factor 2.

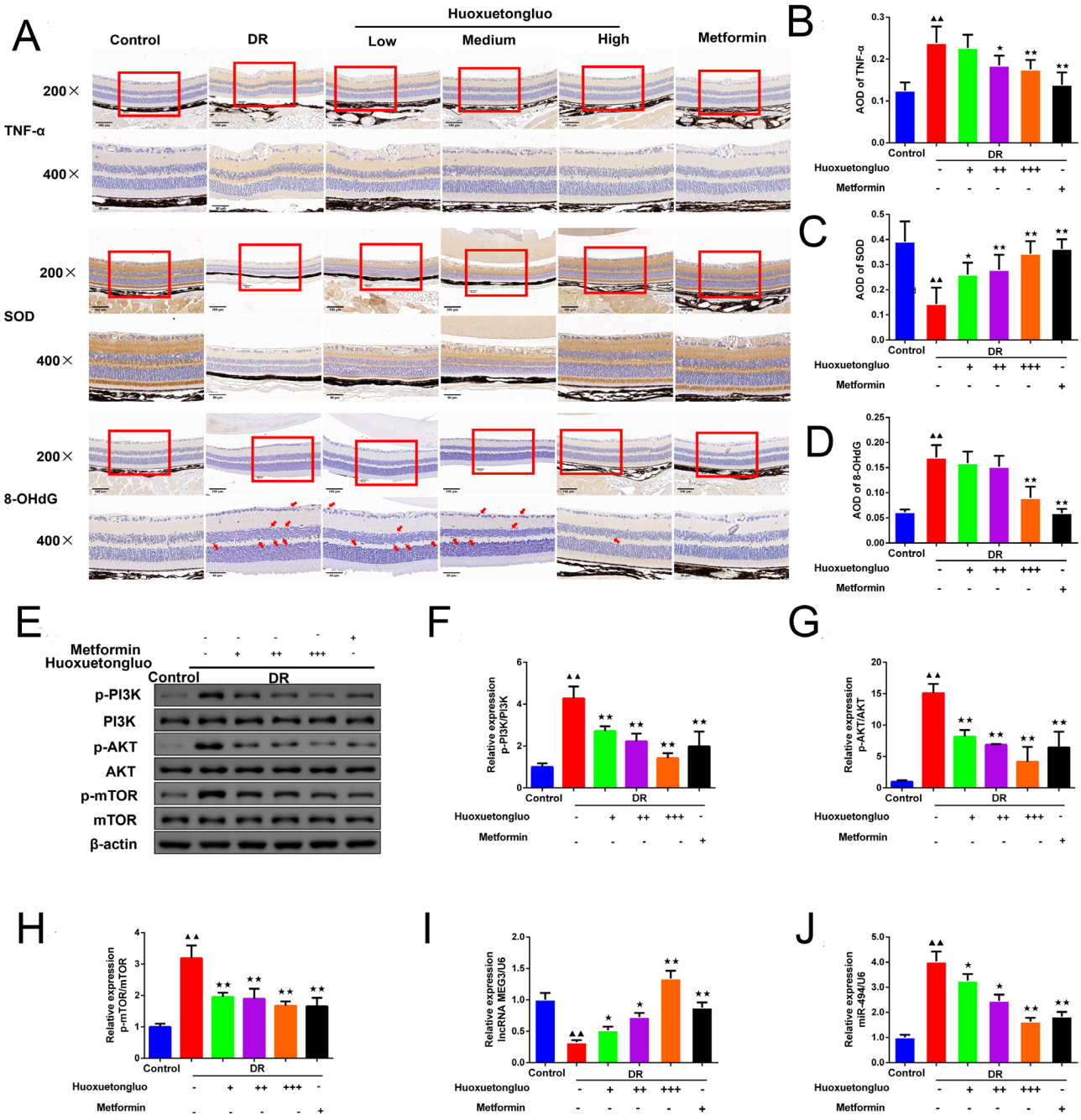


Figure 6. Effects of HXTL on oxidative stress, inflammatory markers, and PI3K/AKT/mTOR pathway in DR mice. **A-D**: The expression levels of TNF-α, SOD, and 8-OHdG in mice retinal tissues detected by IHC. (magnification × 200, scale bar: 100 μm; magnification × 400, scale bar: 50 μm). **E-H**: Western Blot was used for testing the PI3K/AKT/mTOR pathway-related markers level of diabetic retinal tissues in mice, n=3; **I-J**: qRT-PCR was used for testing lncRNA MEG3 and miR-494 levels of mice in each group, n=3; ▲▲p<0.01 versus control group, ★p<0.05, ★★p<0.01 versus DR group. TNF-α: tumor necrosis factor-α, PI3K: phosphoinositol 3 kinase, AKT: protein kinase B, mTOR: mammalian target of rapamycin, lncRNA MEG3: long non-coding RNA maternal imprinting gene 3, miR-494: microRNA-494.

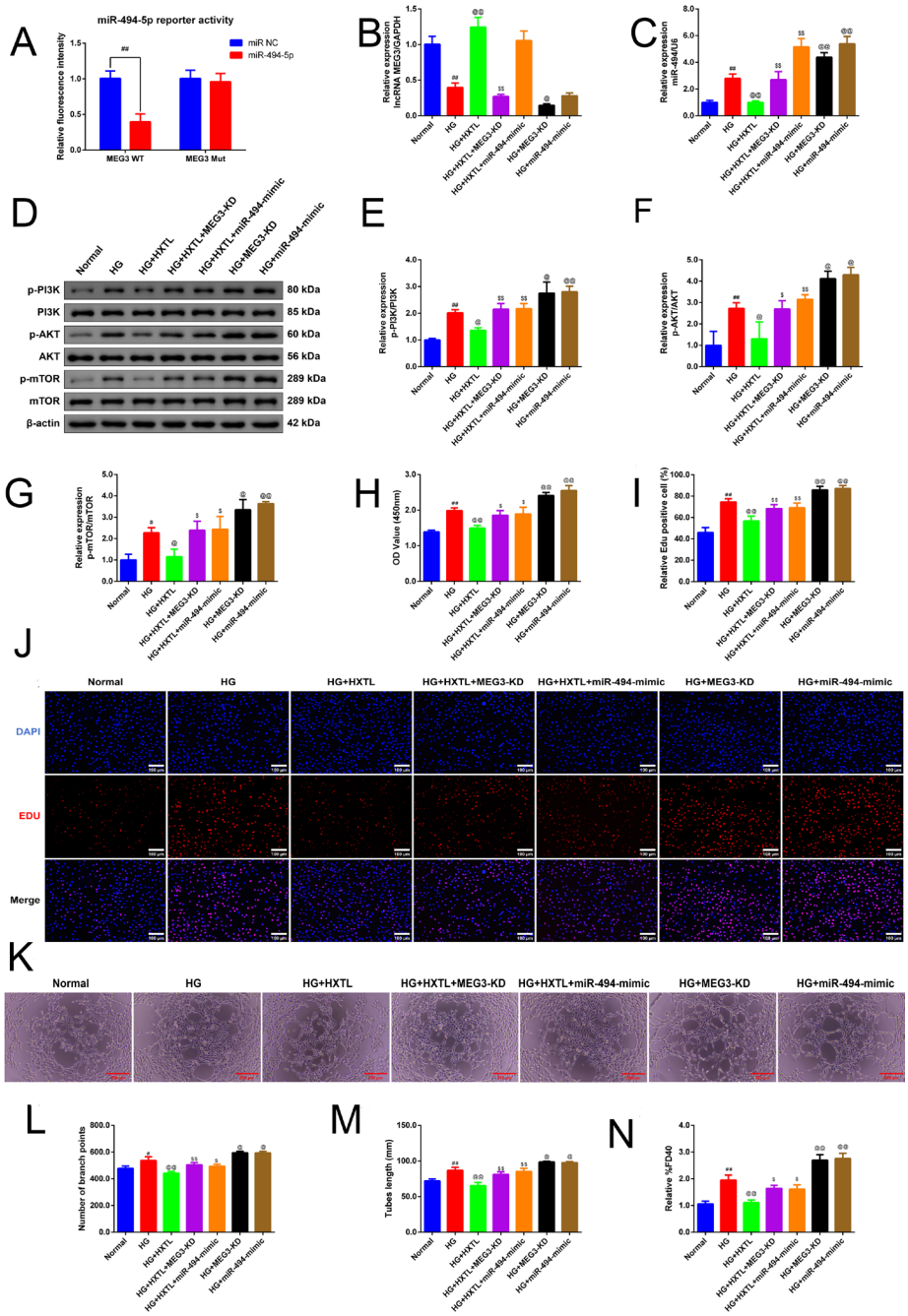


Figure 7. HXTL ameliorates high glucose-induced dysregulation of the MEG3/miR-494–5p axis and PI3K/AKT/mTOR signaling, and alleviates functional impairment in mRMECs. **A**: Dual-luciferase reporter assay confirming the direct targeting of MEG3 by miR-494–5p, n=3; **B**, **C**: Expression levels of lncRNA MEG3 and miR-494–5p in mRMECs under various treatments, n=3; **D**-**G**: Protein expression levels of p-PI3K, p-AKT, and p-mTOR with corresponding quantitative analysis, n=3; **H**: Assessments of cell viability, n=3; **I**-**J**: Assessments of proliferation and quantification of EdU-positive cells, n=3; **K**-**M**: Representative images and quantitative analysis of branch points and tube length from the tube formation assay, n=3; **N**: Endothelial permeability measured by FITC-dextran transendothelial flux, n=3. $^{\#}p<0.05$, $^{\#\#}p<0.01$ versus normal group, $^{@}p<0.05$, $^{@@}p<0.01$ versus HG group; $^{\$}p<0.05$, $^{\$\$}p<0.01$ versus HXTL group. mRMECs: mouse retinal microvascular endothelial cells, Edu: 5-ethynyl-2′-deoxyuridine, FITC: fluorescein isothiocyanate.

lncRNA MEG3 and miR-494. Results showed that HXTL reduced lncRNA MEG3 but increased miR-494 in a dose-dependent manner (Figure 6I-J, $p < 0.05$).

HXTL attenuates high glucose–induced molecular dysregulation and cellular dysfunction via the essential MEG3/miR-494–5p axis: First, we investigated the effects of HXTL on key molecular and functional changes in mRMECs under high-glucose conditions. Dual-luciferase reporter assay confirmed that miR-494–5p directly targets MEG3 (Figure 7A, $p < 0.01$). Compared with the HG group, HXTL treatment reversed the high glucose–induced downregulation of lncRNA MEG3 and upregulation of miR-494–5p (Figure 7B,C, $p < 0.01$). HXTL also significantly suppressed the hyperactivation of the PI3K/AKT/mTOR pathway, as shown by reduced phosphorylation levels of p-PI3K, p-AKT, and p-mTOR (Figure 7D-G, $p < 0.05$). Functionally, HXTL ameliorated high glucose–induced enhancements in cell viability (Figure 7H), proliferation (Figure 7I-J), angiogenic capacity (Figure 7K-M), and endothelial permeability (Figure 7N; all $p < 0.01$).

To clarify the functional necessity of the MEG3/miR-494–5p axis, rescue experiments were performed. Knockdown of MEG3 or overexpression of miR-494–5p significantly counteracted the therapeutic effects of HXTL, leading to reactivation of the PI3K/AKT/mTOR pathway and reappearance of pathologic cellular phenotypes ($p < 0.05$).

DISCUSSION

DR is a common complication of type 2 diabetes related to the fundus microvascular changes, manifested primarily as degenerative visual impairment, including blurred vision and diminished visual acuity. Dyslipidemia and lipid metabolism disorders are prevalent in patients with type 2 diabetes mellitus, and insulin resistance (IR) and insufficient insulin secretion are the main causes. IR leads to reduced lipoprotein lipase synthesis and TG hydrolysis, which in turn leads to lipid metabolism disorders [25,26]. Currently, several clinical drugs are commonly used to control the systemic risk factors of DR, such as hypoglycemic drugs (with metformin being the most well-known and used as a positive control in our study), antihypertension medication, hypolipidemic drugs, medication to correct anemia (erythropoietin), and drugs that protect blood vessels. In our study, we used HXTL, which is composed of *Astragalus*, *chuanxiong*, *Angelica*, *Radix Paeoniae Rubra*, peach kernel, safflower, *S. miltiorrhiza* Bge., *Pueraria*, *Retinervus Luffae Fructus*, *Curcuma*, *Acorus*, leech, motherwort, *L. herba*, and honeysuckle, as a treatment medication. Among these ingredients, the Chinese herb *Panax notoginseng*, *S. miltiorrhiza* Bge., and *Astragalus* served as the main components to improve the cellular metabolism process, inhibit the Hippo signaling pathway, and prevent abnormal angiogenesis [27,28]. Qiming granules, a compound preparation with *Astragalus membranaceus*, *Pueraria*, and wolfberry as main components, also has a certain therapeutic effect on radiation retinopathy [29].

Basic research has found that the HXTL can reduce pancreatic cell damage in db/db mice, improve blood flow in the sciatic nerve area, and promote repair and regeneration of damaged nerves, and its mechanism of action may be related to the improvement of diabetic inflammatory lesions [30]. Preliminary clinical studies have shown that HXTL can alleviate skin abnormal sensations, numbness, and limb pain in patients with diabetic peripheral neuropathy (DPN), as well as improve motor nerve conduction velocity and sensory nerve conduction velocity [31], indicating HXTL is a safe drug used in clinical and basic medical research. In our study, db mice were first treated with HXTL by gavage. The method of gavage also affected the DR mice, as it was noted that certain microbial taxa and related molecular mechanisms may be involved in glucose metabolism associated with diabetes [32,33]. However, we based our results on the same administration to the mice, which had little effect. We found that HXTL can not only effectively reduce the body weight of db/db mice and control blood glucose, but also regulate lipid metabolism and ameliorate pathologic changes in the partial retina, indicating its powerful protective effect against DR. The retina, divided into 10 layers, is a translucent membrane under the naked eye, and it functions as an effective way to transmit light signals into electrical signals. In this study, HE and TUNEL staining revealed that HXTL protected the destroyed structure of retinal tissue and the apoptotic cells. The boundaries of each layer were clear, with little neovascularization, indicating that they improved pathologic changes in retinal tissue. Supporting this, our in vitro experiments in high glucose–stressed mRMECs demonstrated that HXTL treatment significantly alleviated endothelial dysfunction (as evidenced by improved viability, reduced proliferation, attenuated tube formation, and decreased permeability), corroborating its direct protective effects at the cellular level. CD31, also known as platelet endothelial cell adhesion molecule 1 (PECAM-1) [34], is a member of the immunoglobulin superfamily. It is expressed on the surface of vascular endothelial cells, platelets, monocytes, neutrophils, and other cells. VEGFR, a high-affinity receptor that binds specifically to VEGF, is mainly distributed on the endothelial surface of vascular and lymphatic vessels and regulates the generation of blood vessels and lymphatic vessels [35,36]. Retinal neovascularization caused by hyperplasia of retinal blood vessels is a serious eye disease that can lead to vision

loss and blindness. In our study, we found that treatment inhibited vascular hyperplasia by downregulating CD31 and VEGFR expression; at the same time, serum VEGF expression decreased. This indicated that the vascular regeneration was inhibited, and the pathologic structure of the retina was improved by HXTL. Complementing these in vivo observations, tube formation assays in mRMECs under high-glucose conditions revealed that HXTL treatment markedly attenuated angiogenic capacity, further confirming its antiangiogenic property in a controlled cellular model.

Apart from the function of inhibiting new angiogenesis of HXTL, we also found that this medicine inhibited the expressions of inflammatory cytokines IL-1β, IL-6, and TNF-α in retinal tissue and serum. Studies have confirmed the involvement of oxidative stress in the diabetic retina [37]. 3-NT is an important ROS that participates in oxidative stress and is related to cell damage, inflammation, and the production of nitric oxide [38]. 4-HNE [39,40] is an α,β-unsaturated hydroxyl ester of intracellular lipid peroxidation that is readily detected in tissues and blood circulation and is the most studied in oxidative stress. 8-OHdG is an important protein of DNA oxidative damage [41]. SOD is the main biological enzyme scavenging oxygen free radicals in the body and protects cells from oxidative stress [42]. MDA is the end product of lipid metabolism. The more severe the oxidative stress response caused by ischemia and hypoxia, the more obvious the increase in MDA expression is, and its concentration level can reflect the degree of oxidative damage in the body [43,44]. In our study, the expression of 3-NT, 4-HNE, NOX4, VAV2, 8-OHdG, and MDA decreased, while SOD increased after HXTL treatment. These findings suggest that HXTL reduced the oxidative stress damage in the retinal tissue of DR mice. In addition, this study identified multiple active flavonoid and flavonoid glycoside components in HXTL through compositional analysis, including baicalin, naringenin, rutin, and hyperoside. These components were confirmed to have significant anti-inflammatory and antioxidant activities [45–48]. Among them, rutin was also shown to improve lipid metabolism [46]. Our results are consistent with previous studies, indicating that HXTL plays a regulatory role in oxidative stress and inflammation in DR.

The hypoxic-ischemic environment caused by high glucose can activate the expression of AKT in the PI3K/AKT/mTOR signaling pathway in endothelial cells, increase its phosphorylation, and then accelerate the formation of neovascularization. In our study, we found that after the treatment of HXTL in DR mice, the expression of p-PI3K, p-AKT, and p-mTOR was reduced, indicating that the medicine influenced this signaling pathway. Liu et al. reported in their study about ischemic brain injury that reduced lncRNA MEG3 expression level can accelerate angiogenesis [43,49], which is also a key step in the development and progression of DR, suggesting that lncRNA MEG3 may be involved in the occurrence of this disease. MiR-494 is upregulated in myocardial microvascular endothelial cells of diabetic rats [50]. In their study, they hypothesized that miR-494 might be associated with resistin-regulated insulin secretion [51]. Consistent with the findings of previous studies, in our study, we found that when we simulated the diabetic environment in db/db mice, lncRNA MEG3 expression was lower and miR-494 expression was higher in retinal epithelial cells, implying that diabetes could inhibit lncRNA MEG3 and increase miR-494 expressions with high blood glucose levels; hence, with the interference of HXTL, it upregulated lncRNA MEG3 and restrained miR-494. In this study, we demonstrated that HXTL changed the DR in mice at different dosages, with upregulation of lncRNA MEG3 restraining miR-494 and inhibiting PI3K/AKT/mTOR pathway. This regulatory effect was further confirmed in high glucose–treated mRMECs, where HXTL restored the balance of MEG3/miR-494–5p and subsequently inhibited the activation of the PI3K/AKT/mTOR pathway, highlighting a consistent mechanism across experimental models.

Currently, in clinical treatment, HXTL has been proven to have significant efficacy in diabetic complications, covering conditions such as DPN and diabetic nephropathy [52]. Therefore, HXTL has great potential for development as a DR therapeutic drug. It has shown good therapeutic effects in animal models and has multiple mechanisms of action, such as modulating inflammatory responses and improving vascular function. The findings of this study not only lay a solid experimental foundation for the further clinical application of HXTL but also provide a basis for the clinical practice of traditional Chinese medicine in the field of DR treatment.

Despite the promising findings, several limitations of the present study should be acknowledged. First, the relatively short treatment duration may not fully capture the long-term therapeutic effects of HXTL in diabetic retinopathy. Future investigations involving extended treatment periods are warranted to evaluate the sustainability of its protective actions. Second, although we have demonstrated the involvement of the MEG3/miR-494–5p axis in mediating the effects of HXTL, the precise molecular mechanisms underlying their regulation in DR remain incompletely understood. Further studies are needed to elucidate the downstream targets and signaling networks modulated by this axis. Finally, while our preclinical data provide a solid foundation, translational research, including well-designed clinical trials, is essential

to validate the safety and efficacy of HXTL in human patients with diabetic retinopathy.

In summary, HXTL contains 181 identified constituents and alleviates DR in db/db mice by reducing body weight, blood glucose, retinal damage, oxidative stress, inflammation, and pathologic angiogenesis. In vitro, it restores MEG3/miR-494–5p balance, inhibits PI3K/AKT/mTOR signaling, and improves endothelial function. Mechanistically, its protective effects are mediated through the MEG3/miR-494–5p axis. These results demonstrate the therapeutic potential of HXTL and provide a foundation for clinical development.

APPENDIX 1. SUPPLEMENTARY TABLE 1.

To access the data, click or select the words "Appendix 1." Attributed chemical composition in positive ion mode.

APPENDIX 2. SUPPLEMENTARY TABLE 2.

To access the data, click or select the words "Appendix 2." Attributed chemical composition in negative ion mode

ACKNOWLEDGMENTS

Ethical considerations: All procedures involving animals were approved by the animal research was ratified by the Ethics Committee of the Animal Center of Zhejiang Eyong Pharmaceutical Research and Development Center. Animal use license number: SYXK (Zhe) 2021–0033. Declaration of conflicting interest: The authors declared no potential conflicts of interest with respect to the research, authorship, and/or publication of this article. Funding statement: This work was supported by [Zhejiang Provincial Public Service and Application Research Foundation] (Grant number LGF21H120001) and [Zhejiang Traditional Medicine and Technology Program] (Grant number 2025ZL082). Data availability: The data sets generated during and/or analyzed during the current study are available from the corresponding author on reasonable request. Author Contributions: Study conception by Jian Lai and Neng Li; acquisition of data by Neng Li, Jian Lai and Lin Zhu; Statistical analysis by Neng Li and Lin Zhu; manuscript draft by Neng Li, Lin Zhu; manuscript revision by Jian Lai.

This is an open-access article distributed under the terms of the Creative Commons Attribution-NonCommercial-NoDerivatives 4.0 International License, which permits reusers to copy and distribute the material in any medium or format in unadapted form only, for noncommercial purposes only, and only so long as attribution is given to the creator. CC BY-NC-ND includes the following elements: BY: credit must be given to the creator. NC: Only noncommercial uses of the work are permitted. ND: No derivatives or adaptations of the work are permitted.

REFERENCES

1. Wu L, Acón D, Wu A, Wu M. Vascular endothelial growth factor inhibition and proliferative diabetic retinopathy, a changing treatment paradigm? Taiwan J Ophthalmol 2019; 9:216-23. [PMID: 31942426].
2. Kalogeropoulos D, Kalogeropoulos C, Stefaniotou M, Neofytou M. The role of tele-ophthalmology in diabetic retinopathy screening. J Optom 2020; 13:262-8. [PMID: 31948924].
3. Cabrera AP, Monickaraj F, Rangasamy S, Hobbs S, McGuire P, Das A. Do Genomic Factors Play a Role in Diabetic Retinopathy? J Clin Med 2020; 9:216-[PMID: 31947513].
4. Cecilia OM, José Alberto CG, José NP, Ernesto Germán CM, Ana Karen LC, Luis Miguel RP, Ricardo Raúl RR, Adolfo Daniel RC. Oxidative Stress as the Main Target in Diabetic Retinopathy Pathophysiology. J Diabetes Res 2019; 2019:8562408[PMID: 31511825].
5. Kovoor E, Chauhan SK, Hajrasouliha A. Role of inflammatory cells in pathophysiology and management of diabetic retinopathy. Surv Ophthalmol 2022; 67:1563-73. [PMID: 35914582].
6. Kupis M, Samelska K, Szaflik J, Skopiński P. Novel therapies for diabetic retinopathy. Cent Eur J Immunol 2022; 47:102-8. [PMID: 35600148].
7. Chou Y, Ma J, Su X, Zhong Y. Emerging insights into the relationship between hyperlipidemia and the risk of diabetic retinopathy. Lipids Health Dis 2020; 19:241-[PMID: 33213461].
8. Tomkins-Netzer O, Niederer R, Lightman S. The role of statins in diabetic retinopathy. Trends Cardiovasc Med 2024; 34:128-35. [PMID: 36464210].
9. Maugeri G, Bucolo C, Drago F, Rossi S, Di Rosa M, Imbesi R, D'Agata V, Giunta S. Attenuation of High Glucose-Induced Damage in RPE Cells through p38 MAPK Signaling Pathway Inhibition. Front Pharmacol 2021; 12:684680[PMID: 34025440].
10. Yang J, Liu Z. Mechanistic Pathogenesis of Endothelial Dysfunction in Diabetic Nephropathy and Retinopathy. Front Endocrinol (Lausanne) 2022; 13:816400[PMID: 35692405].
11. Chang WW, Zhang L, Yao XM, Chen Y, Zhu LJ, Fang ZM, Zhao Y, Yao YS, Jin YL. Upregulation of long non-coding RNA MEG3 in type 2 diabetes mellitus complicated with vascular disease: a case-control study. Mol Cell Biochem 2020; 473:93-9. [PMID: 32594338].
12. Tu Y, Zhu M, Wang Z, Wang K, Chen L, Liu W, Shi Q, Zhao Q, Sun Y, Wang X, Song E, Liu X. Melatonin inhibits Müller cell activation and pro-inflammatory cytokine production via upregulating the MEG3/miR-204/Sirt1 axis in experimental diabetic retinopathy. J Cell Physiol 2020; 235:8724-35. [PMID: 32324260].

13. Perisset S, Potilinski MC, Gallo JE. Role of Lnc-RNAs in the Pathogenesis and Development of Diabetic Retinopathy. Int J Mol Sci 2023; 24:13947-[PMID: 37762249].

14. Zhang ZZ, Qin XH, Zhang J. MicroRNA-183 inhibition exerts suppressive effects on diabetic retinopathy by inactivating *BTG1*-mediated PI3K/Akt/VEGF signaling pathway. Am J Physiol Endocrinol Metab 2019; 316:E1050-60. [PMID: 30835506].

15. Lu JM, Zhang ZZ, Ma X, Fang SF, Qin XH. Repression of microRNA-21 inhibits retinal vascular endothelial cell growth and angiogenesis via PTEN dependent-PI3K/Akt/VEGF signaling pathway in diabetic retinopathy. Exp Eye Res 2020; 190:107886[PMID: 31759996].

16. Zhao Y. Effect of Yiqi Huoxue Tongluo Decoction on blood glucose level and serum cystatin C in diabetic patients. Zhong Yao Cai 2018; 41:734-6. .

17. Li X, Shi F, Zhang R, Sun C, Gong C, Jian L, Ding L. Pharmacokinetics, Safety, and Tolerability of Amygdalin and Paeoniflorin After Single and Multiple Intravenous Infusions of Huoxue-Tongluo Lyophilized Powder for Injection in Healthy Chinese Volunteers. Clin Ther 2016; 38:327-37. [PMID: 26749220].

18. Lós DB, Oliveira WH, Duarte-Silva E, Sougey WWD, Freitas EDSR, de Oliveira AGV, Braga CF, França MER, Araújo SMDR, Rodrigues GB, Rocha SWS, Peixoto CA, Moraes SRA. Preventive role of metformin on peripheral neuropathy induced by diabetes. Int Immunopharmacol 2019; 74:105672[PMID: 31195189].

19. Han YC, Tang SQ, Liu YT, Li AM, Zhan M, Yang M, Song N, Zhang W, Wu XQ, Peng CH, Zhang H, Yang S. AMPK agonist alleviate renal tubulointerstitial fibrosis via activating mitophagy in high fat and streptozotocin induced diabetic mice. Cell Death Dis 2021; 12:925-[PMID: 34628484].

20. Zhang W, Zhang D, Cheng Y, Liang X, Wang J. Runx1 regulates Tff1 expression to expedite viability of retinal microvascular endothelial cells in mice with diabetic retinopathy. Exp Eye Res 2022; 217:108969[PMID: 35114215].

21. Gu X, Long Q, Wei W, Tong J, Li Z, Zhang Z, Jiao Y. Number 2 Feibi Recipe Inhibits H_2O_2-Mediated Oxidative Stress Damage of Alveolar Epithelial Cells by Regulating the Balance of Mitophagy/Apoptosis. Front Pharmacol 2022; 13:830554[PMID: 35370684].

22. Fan X, Huang H, Ji Z, Mao Q. Long non-coding RNA MEG3 functions as a competing endogenous RNA of miR-93 to regulate bladder cancer progression via PI3K/AKT/mTOR pathway. Transl Cancer Res 2020; 9:1678-88. [PMID: 35117516].

23. Zhang H, Li J. Protective Effects of Propofol on Acute Kidney Injury Through Suppressing Ferroptosis and Inflammatory Responses in Renal Tubular Epithelial Cells. Discov Med 2025; 37:3095-.

24. Jiang J, Dong W, Zhang W, Wang Q, Wang R, Wang J, Wu H, Dong H, Zhao RC, Wang J, Li Z. LncRNA *SLC1A5-AS/MZF1/ASCT2* Axis Contributes to Malignant Progression of Hepatocellular Carcinoma. Discov Med 2023; 35:995-1014. [PMID: 38058065].

25. Wang X, Long D, Hu X, Guo N. Gentiopicroside modulates glucose homeostasis in high-fat-diet and streptozotocin-induced type 2 diabetic mice. Front Pharmacol 2023; 14:1172360[PMID: 37601073].

26. Dewidar B, Mastrototaro L, Englisch C, Ress C, Granata C, Rohbeck E, Pesta D, Heilmann G, Wolkersdorfer M, Esposito I, Reina Do Fundo M, Zivehe F, Yavas A, Roden M. Alterations of hepatic energy metabolism in murine models of obesity, diabetes and fatty liver diseases. EBioMedicine 2023; 94:104714[PMID: 37454552].

27. Hao GM, Lv TT, Wu Y, Wang HL, Xing W, Wang Y, Li C, Zhang ZJ, Wang ZL, Wang W, Han J. The Hippo signaling pathway: a potential therapeutic target is reversed by a Chinese patent drug in rats with diabetic retinopathy. BMC Complement Altern Med. 2017;17:187.

28. Sun HH, Chai XL, Li HL, Tian JY, Jiang KX, Song XZ, Wang XR, Fang YS, Ji Q, Liu H, Hao GM, Wang W, Han J. Fufang Xueshuantong alleviates diabetic retinopathy by activating the PPAR signalling pathway and complement and coagulation cascades. J Ethnopharmacol 2021; 265:113324[PMID: 32890714].

29. Huang Y, Wang J, Wang Y, Kuang W, Xie M, Zhang M. Pharmacological mechanism and clinical study of Qiming granules in treating diabetic retinopathy based on network pharmacology and literature review. J Ethnopharmacol 2023; 302:Pt A115861[PMID: 36332761].

30. Yao YSG, Jiang A, Wang L, Ye S, Wang L. Influence of Yiqi Huoxue Tongluo Fang on JNK signal pathway and inflammatory factors in mice with diabetic peripheral neuropathy. J Beijing Univ Tradit Chin Med 2017; 40:923-7. .

31. Lin YWF, Li J, Ruan N, Fang Z, Shen G. Therapeutic effect of Yiqi Huoxue Tongluo Fang on diabetic peripheral neuropathy. Clin J Tradit C Med 2019; 31:2135-8. .

32. Gurung M, Li Z, You H, Rodrigues R, Jump DB, Morgun A, Shulzhenko N. Role of gut microbiota in type 2 diabetes pathophysiology. EBioMedicine 2020; 51:102590[PMID: 31901868].

33. Crudele L, Gadaleta RM, Cariello M, Moschetta A. Gut microbiota in the pathogenesis and therapeutic approaches of diabetes. EBioMedicine 2023; 97:104821[PMID: 37804567].

34. Wu Q, Du X, Cheng J, Qi X, Liu H, Lv X, Gong X, Shao C, Wang M, Yue L, Yang X, Li S, Zhang Y, Li X, Yang H. PECAM-1 drives β-catenin-mediated EndMT via internalization in colon cancer with diabetes mellitus. Cell Commun Signal 2023; 21:203-[PMID: 37580771].

35. Uemura A, Fruttiger M, D'Amore PA, De Falco S, Joussen AM, Sennlaub F, Brunck LR, Johnson KT, Lambrou GN, Rittenhouse KD, Langmann T. VEGFR1 signaling in retinal angiogenesis and microinflammation. Prog Retin Eye Res 2021; 84:100954[PMID: 33640465].

36. Florek K, Mendyka D, Gomułka K. Vascular Endothelial Growth Factor (VEGF) and Its Role in the Cardiovascular System. Biomedicines 2024; 12:1055-[PMID: 38791016].

37. Hsu YJ, Lin CW, Cho SL, Yang WS, Yang CM, Yang CH. Protective Effect of Fenofibrate on Oxidative Stress-Induced Apoptosis in Retinal-Choroidal Vascular Endothelial Cells: Implication for Diabetic Retinopathy Treatment. Antioxidants (Basel) 2020; 9:712-[PMID: 32764528].

38. Bódi B, Kovács Á, Gulyás H, Mártha L, Tóth A, Mátyás C, Barta BA, Oláh A, Merkely B, Radovits T, Papp Z. Long-Term PDE-5A Inhibition Improves Myofilament Function in Left and Right Ventricular Cardiomyocytes through Partially Different Mechanisms in Diabetic Rat Hearts. Antioxidants (Basel) 2021; 10:1776-[PMID: 34829647].

39. Abouhish H, Thounaojam MC, Jadeja RN, Gutsaeva DR, Powell FL, Khriza M, Martin PM, Bartoli M. Inhibition of HDAC6 Attenuates Diabetes-Induced Retinal Redox Imbalance and Microangiopathy. Antioxidants (Basel) 2020; 9:599-[PMID: 32660051].

40. Jaganjac M, Milkovic L, Zarkovic N, Zarkovic K. Oxidative stress and regeneration. Free Radic Biol Med 2022; 181:154-65. [PMID: 35149216].

41. Urbaniak SK, Boguszewska K, Szewczuk M, Kaźmierczak-Barańska J, Karwowski BT. 8-Oxo-7,8-Dihydro-2′-Deoxyguanosine (8-oxodG) and 8-Hydroxy-2′-Deoxyguanosine (8-OHdG) as a Potential Biomarker for Gestational Diabetes Mellitus (GDM) Development. Molecules 2020; 25:202-[PMID: 31947819].

42. Saxena P, Selvaraj K, Khare SK, Chaudhary N. Superoxide dismutase as multipotent therapeutic antioxidant enzyme: Role in human diseases. Biotechnol Lett 2022; 44:1-22. [PMID: 34734354].

43. Zhang Z, Qin X, Wang Z, Li Y, Chen F, Chen R, Li C, Zhang W, Zhang M. Oxymatrine pretreatment protects H9c2 cardiomyocytes from hypoxia/reoxygenation injury by modulating the PI3K/Akt pathway. Exp Ther Med 2021; 21:556-[PMID: 33850528].

44. Huang J, Liu Y, Wang M, Wang R, Ling H, Yang Y. FoxO4 negatively modulates USP10 transcription to aggravate the apoptosis and oxidative stress of hypoxia/reoxygenation-induced cardiomyocytes by regulating the Hippo/YAP pathway. J Bioenerg Biomembr 2021; 53:541-51. [PMID: 34251583].

45. Pan L, Cho KS, Yi I, To CH, Chen DF, Do CW. Baicalein, Baicalin, and Wogonin: Protective Effects against Ischemia-Induced Neurodegeneration in the Brain and Retina. Oxid Med Cell Longev 2021; 2021:8377362[PMID: 34306315].

46. Liu Y, Sun Z, Dong R, Liu P, Zhang X, Li Y, Lai X, Cheong HF, Wu Y, Wang Y, Zhou H, Gui D, Xu Y. Rutin ameliorated lipid metabolism dysfunction of diabetic NAFLD via AMPK/SREBP1 pathway. Phytomedicine 2024; 126:155437[PMID: 38394735].

47. Valle-Velázquez E, Zambrano-Vásquez OR, Cortés-Camacho F, Sánchez-Lozada LG, Guevara-Balcázar G, Osorio-Alonso H. Naringenin - a potential nephroprotective agent for diabetic kidney disease: A comprehensive review of scientific evidence. Biomol Biomed 2024; 24:1441-51. [PMID: 38907737].

48. Zhang K, Li M, Yin K, Wang M, Dong Q, Miao Z, Guan Y, Wu Q, Zhou Y. Hyperoside mediates protection from diabetes kidney disease by regulating ROS-ERK signaling pathway and pyroptosis. Phytother Res 2023; 37:5871-82. [PMID: 37646382].

49. Liu J, Li Q, Zhang KS, Hu B, Niu X, Zhou SM, Li SG, Luo YP, Wang Y, Deng ZF. Downregulation of the Long Non-Coding RNA Meg3 Promotes Angiogenesis After Ischemic Brain Injury by Activating Notch Signaling. Mol Neurobiol 2017; 54:8179-90. [PMID: 27900677].

50. Wang XH, Qian RZ, Zhang W, Chen SF, Jin HM, Hu RM. MicroRNA-320 expression in myocardial microvascular endothelial cells and its relationship with insulin-like growth factor-1 in type 2 diabetic rats. Clin Exp Pharmacol Physiol 2009; 36:181-8. [PMID: 18986336].

51. Wen F, Yang Y, Sun C, Fang H, Nie L, Li L, Liu Y, Yang Z. RESISTIN INHIBITS GLUCOSE-STIMULATED INSULIN SECRETION THROUGH MIR-494 BY TARGET ON STXBP5. Acta Endocrinol (Buchar) 2017; 13:32-9. [PMID: 31149145].

52. Li B, Lijian D. Research Progress on Pharmacological Action and Clinical Application of Huoxue Tongluo Formula. Clin Misdiagnose Mistreatment. 2023; 36:148-52. .

Articles are provided courtesy of Emory University and The Abraham J. & Phyllis Katz Foundation. The print version of this article was created on 12 September 2026. This reflects all typographical corrections and errata to the article through that date. Details of any changes may be found in the online version of the article.